Numerical comparison of grid pattern diffraction effects through measurement and modeling with OptiScan software

Ian B. Murray[*a], Victor Densmore[b], Vaibhav Bora[b],
Matthew W. Pieratt[a], Douglas L. Hibbard[a], Tom D. Milster[b]
[a]Exotic Electro-Optics, 36570 Briggs Road, Murrieta, CA, USA 92563;
[b]University of Arizona, 1630 East University Boulevard, Tucson, Arizona, 85721

ABSTRACT

Coatings of various metalized patterns are used for heating and electromagnetic interference (EMI) shielding applications. Previous work has focused on macro differences between different types of grids, and has shown good correlation between measurements and analyses of grid diffraction. To advance this work, we have utilized the University of Arizona's OptiScan software, which has been optimized for this application by using the Babinet Principle. When operating on an appropriate computer system, this algorithm produces results hundreds of times faster than standard Fourier-based methods, and allows realistic cases to be modeled for the first time. By using previously published derivations by Exotic Electro-Optics, we compare diffraction performance of repeating and randomized grid patterns with equivalent sheet resistance using numerical performance metrics. Grid patterns of each type are printed on optical substrates and measured energy is compared against modeled energy.

Keywords: grid, diffraction, shielding effectiveness, mesh, OptiScan, Babinet, sheet resistance, hub and spoke

1. INTRODUCTION

Since mesh grids of various types and patterns are often used for heating and electromagnetic interference (EMI) shielding, transmission and shielding has been studied analytically[1] and through measurement [2-4], even for grids placed on either side of a window[5]. This existing work has shown that open area is a reliable indicator of transmission for all types of grids, and that repeating circular patterns appear to have less intense diffracted patterns.

The purpose of this paper is to extend the closed-form calculations and simple experiments to allow optimization of different types of grid patterns. Repeating and randomized patterns are analyzed to show the differences and advantages of each of the pattern types, and measurements are used to reinforce modeling predictions.

1.1 Patterns evaluated

Proprietary software was created at EEO to digitally produce grid patterns in various image and data formats based on desired parameters. Grid patterns with similar characteristics to those described in previous publications were modeled as part of the initial model validation. Figure 1 shows a square grid pattern with linewidths and spacings equivalent to Table 1 and 2 of reference [1], and Figure 2 shows circular patterns with spacing/diameter ratios of 2/3 and 1.6, which is equivalent to those used in reference [3].

To optimize each of these general patterns, the software allowed the following parameters to be varied:

- Spacing (g) and spacing randomization;
- Linewidth (2a) and linewidth randomization;
- Diameter (2R) and diameter randomization for the overlapping circle pattern.

[*] imurray@exotic-eo.com; phone 1 951 926-7618; exotic-eo.com
Ian B. Murray, EEO; Victor Densmore, UA; Vaibhav Bora, UA; Matthew W. Pieratt, EEO; Douglas L. Hibbard, EEO; Tom D. Milster, UA; "Numerical comparison of grid pattern diffraction effects through measurement and modeling with OptiScan software", Window and Dome Technologies and Materials XII, Randal W. Tustison, Volume 8016, Page 80160U, 2011,
http://dx.doi.org/10.1117/12.883422

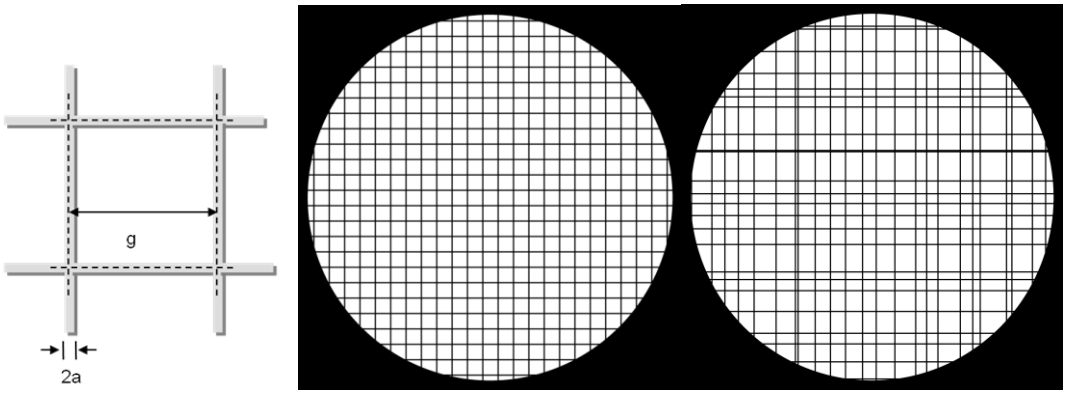

Figure 1 Repeating square grid pattern defined (left). The center image shows a repeating grid pattern, and the right image shows one instance of 50% randomization using grid parameters of 2a=20µm, g=250µm, and sheet resistance of 12.5 Ω/□. A circular aperture is placed over the grid for comparison against reference [1].

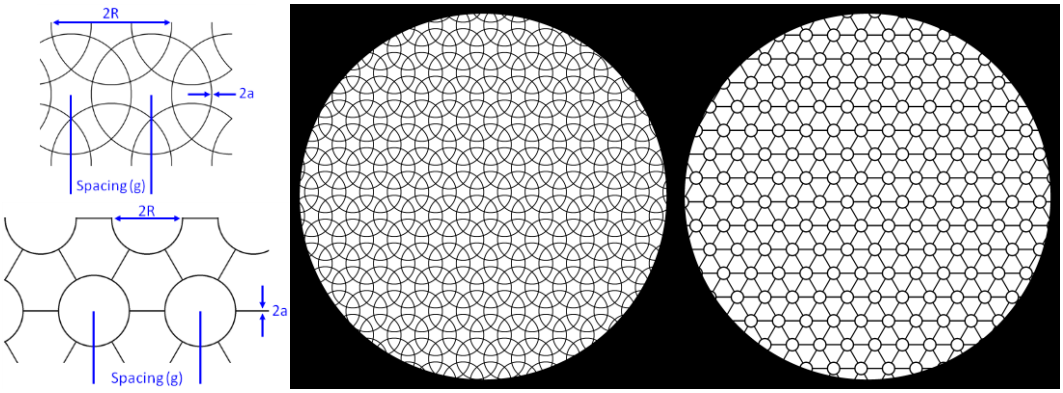

Figure 2 Circular patterns defined (left). An overlapping circle pattern is shown (center) with a g/2R ratio of 2/3 (2a=14.47µm, g=446.3µm, and 2R=669.5µm), and a hub-and-spoke pattern is shown with a g/2R ratio of 2.23 (2a=21.05µm, g=446.3µm, and 2R=200µm). Sheet resistance for both patterns is 12.5 Ω/□.

1.2 Sheet resistance of pattern types

To ensure that equivalent patterns are compared, relative comparisons between pattern types use equivalent patterned sheet resistance as described in references [2] and [6]. This is performed by assuming an unpatterned sheet resistance of 1 Ω/□ so that the results are independent of grid height (stack height) and the bulk metal resistivity. Transmission at non-normal angles of incidence was not modeled, so grid height does not affect any of the following results. Shielding effectiveness is generally well-correlated to sheet resistance for realistic grid patterns [2].

2. APPROACH

2.1 OptiScan software and Babinet engine

Propagation of light from a source plane to an observation plane can be divided into a sequence of smaller calculations that propagate individual components of the source plane. These separate calculations are then added to form the equivalent single-step propagation. In this work, a Babinet technique is used to calculate diffraction patterns instead of using fast Fourier transforms (FFTs). The Babinet technique uses a piece-wise method, where the diffraction integral is approximated with a finite sum of individual calculations.

The basic geometry of the problem is shown in Fig. 3, where diffraction from the source is calculated on an area at the observation screen. The advantage of a piece-wise calculation is that any observation area may be chosen at arbitrary sampling. Therefore, fine sampling of diffraction patterns can be investigated without the need for large matrices. In

addition, true source propagation can be accomplished, without zero padding FFTs or assuming an infinitely periodic object. The penalty for not using FFTs is that computation time for the total calculation is longer.

The approach used in this work starts with decomposing the source field by Babinet's Principle into a finite sum of square windows, where each window is the size of a sampling period. The observation field is assumed to be in the Fraunhofer zone of each individual source window. If pixel (x_{sp}, y_{sp}) has dimensions Δ_{sx} and Δ_{sy} in the *x* and *y* directions, respectively, distance to the observation plane must be at least

$$(z_0)_{\min} = 100\frac{\max\left[\Delta_{sx}\,\Delta_{sy}\right]^2}{\lambda}, \tag{1}$$

where max[] is the maximum and λ is wavelength. Detailed sampling and other considerations are discussed in reference [7]. Typically, Eq. (1) is accomplished through discretization of the source plane into a fine square mesh. In the Babinet code written for this application, a constant size is assumed for Δ_{sx} and Δ_{sy}. That is, Δ_{sx}= Δ_{sy}= Δ. Also, distance z_0 from the source plane to the observation plane is a constant for all pixels. Neither of these restrictions is fundamental, and the code is straightforward to implement that would allow flexible source pixel size and observation-plane spacing.

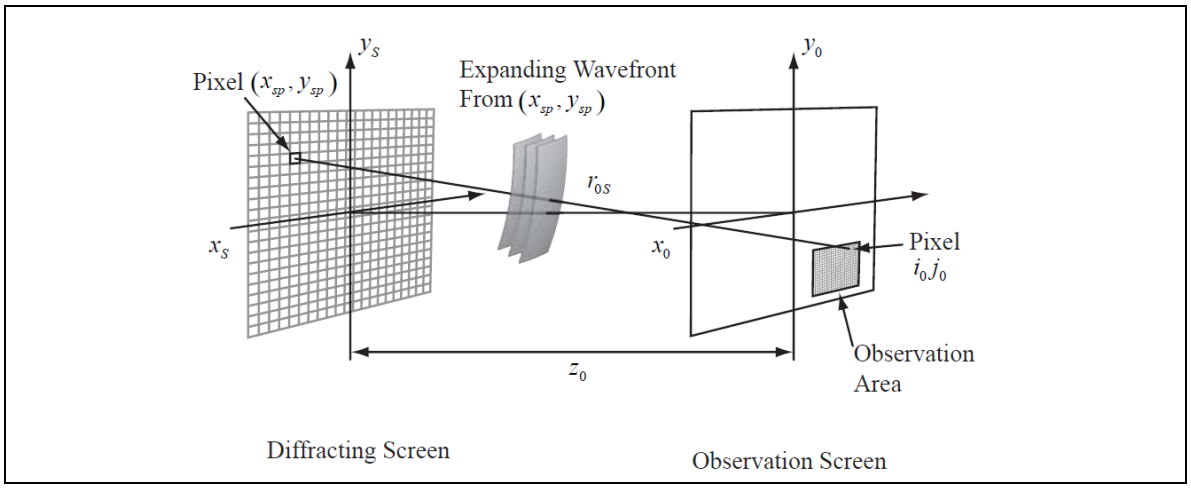

Figure 3 Piece-wise diffraction.

The algorithm only calculates non-zero input pixels, N_{nz}. The number of output pixels N_{out} is determined from the output matrix size. The total number of calculation units is N_{nz}*N_{out}.

To address the computation time penalty, the software was optimized to take advantage of Graphical Processing Unit (GPU) boards. Performance tests utilized files with non-zero elements ranging from 3000 to 810,000 and 1024^2 output pixels, and showed that a single GPU environment decreased computation time by 80 compared to a single-processor environment. This factor is not significantly dependent of the size of the input array, although there is a small penalty for smaller input files due to the larger relative portion of overhead. The multiple-GPU environment is by far the fastest engine, with a speedup factor of over 1000, although again there is a penalty for smaller input files due to overhead.

2.2 Comparison of algorithm against previous work

Reference [1] describes the theoretical diffraction from square mesh grids and derived two equations that can be readily checked using the OptiScan algorithms. The angle of the diffracted orders is predicted by (equation 24 in reference [1]):

$$\sin\theta_x = \frac{n\lambda}{g} \cong \theta_x. \tag{3}$$

The energy in a diffracted order is given by (equation 22 in reference [1]):

$$\frac{\text{energy in order } (n,m) \text{ with mesh}}{\text{energy in PSF without mesh}} = \frac{(g-2a)^4}{g^4}\,\text{sinc}^2\left[\frac{n(g-2a)}{g}\right]\text{sinc}^2\left[\frac{m(g-2a)}{g}\right] \tag{4}$$

Equation (3) predicts that for a repeating square grid pattern with parameters provided in Table 1 of the reference (g = 250µm, λ = 1µm, 2a = 20µm), the orders should be separated by 0.2292°. Figure 4 shows that energy in each of the orders computed by the OptiScan algorithm is within 1% of theory, and the peak location is within 0.1% of theory.

The differences in peak energies compared are likely due to the fact that the theory assumes that each diffracted order is a delta function and the energy from one order does not overlap with the energy from another order – but as can be seen in Figure 5, even a very small Airy disk will affect the energies in the diffracted orders. Taking this into account, the match of the absolute energy in the diffracted orders is considered to be very good.

More complex patterns like hub-and-spoke patterns are much more difficult to analyze theoretically, but reference [3] has shown that transmission at normal incidence can be predicted from the open area for any type of pattern. To demonstrate this effect, the repeating hub-and-spoke pattern shown in Figure 2 was analyzed (open area of 84.1%, which predicts a transmission of 70.7%). Using the same settings as for the square grid, the energy in the primary peak was found to be 70.4%, which again is within 1% of theory and considered to be a good match.

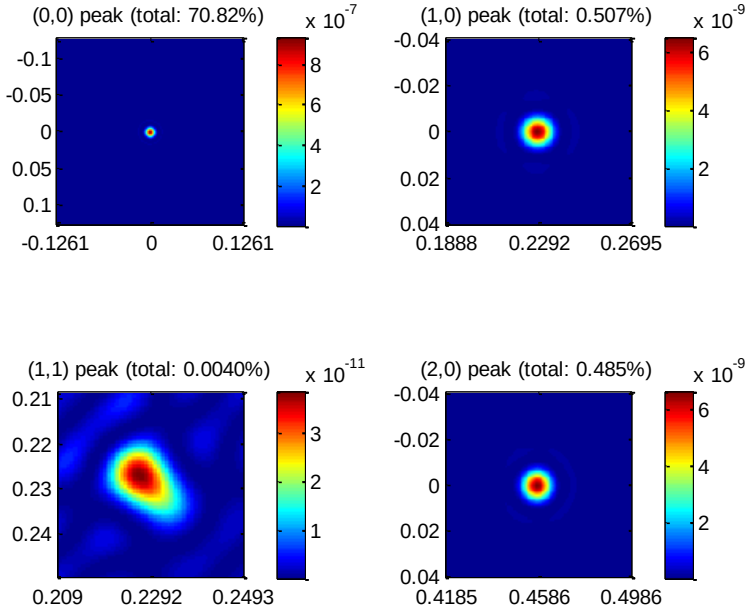

Figure 4 Peaks for diffracted orders [0,0] (top left), [1,0] (top right), [2,0] (bottom right) and [1,1] (bottom left) of a repeating square grid. The orders are expected to be located 0.2292° apart, and expected energy values per the reference are 71.64%, 0.530%, 0.498%, and 0.0039%, respectively. Differences in peak energies from the theoretical values are due to the effects of the aperture diffraction on each of the peaks.

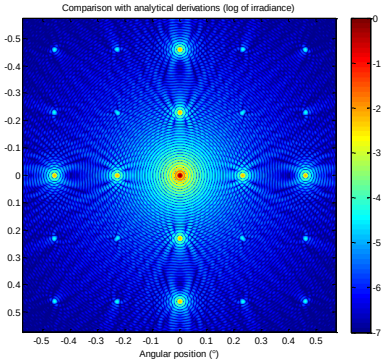

Figure 5 Diffraction of a square grid with g = 250µm, 2a = 20µm, λ = 1µm, and sheet resistance of 12.5 Ω/□. Note that the Airy disk pattern from the primary peak has a clear impact on the diffracted peaks.

2.3 Diffraction pattern noise metric

To compare diffraction of grids, simply looking at the magnitude of peaks relative to each other is not considered adequate, since realistic systems pixelate the image and may be less sensitive to a peak that spreads across several detector pixels than a peak entirely contained within one detector pixel.

The noise metric analyzes diffraction patterns in the following manner:

1. Use a pixel pitch equal to the Airy disk diameter.
2. Find the energy in the zero-order peak pixel (center the pixel on the peak of the Airy disk).
3. Ignore pixels with signal primarily due to the zero-order peak (ignore a region equal to half the distance between the zero-order peak and the surrounding first-order peaks).
4. Find "noise" signal in all other pixels by scanning a grid across image in a raster pattern to find the location of the maximum noise pixel. The raster pattern uses steps in both axes equal to 1/20th of the larger pixel size.

The resulting metric value is computed as:

$$Pixelated\ noise\ metric = \frac{Maximum\ signal\ of\ a\ noise\ pixel}{Signal\ of\ the\ (0,0)\ pixel}$$

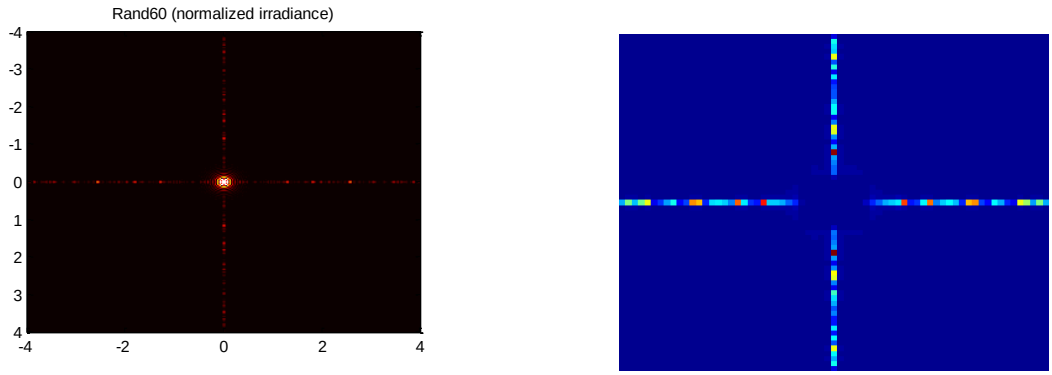

Figure 6 The diffracted pattern on the left is pixelated and, after the zero-order signal is calculated, the center energy is ignored. The image on the right is one raster case showing that each pixel is equal to the Airy disk diameter of the image on the left, and that the central peak is ignored to a distance of half of the distance to the first-order primary peak – roughly equivalent to 5 times the Airy disk diameter in this example.

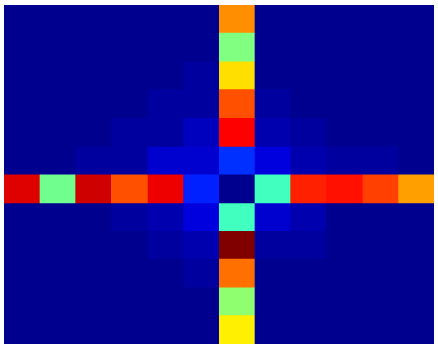

Figure 7 An alternative metric is to pixelate the diffracted pattern into larger pixels. This image uses pixels that are 3.9x larger than in the normal metric.

3. ANALYSIS

3.1 Square grid diffraction

Although repeating square patterns have strong higher-order diffraction peaks, random square patterns can reduce the energy in the diffraction peak by several orders of magnitude. Figure 8 shows this effect qualitatively.

Using the metric described in the section 2.3, random square patterns (created with similar parameters as those used in reference [2]) were compared quantitatively to see how randomization can improve undesired diffraction. Figure 9 shows that, once 50% randomization has been reached, further randomization does not consistently result in less diffracted noise. It also shows that randomization can improve the diffracted noise by a factor of 5.25, which is a considerable improvement, resulting in a pixel with a signal of only 0.23% of the signal in the zero-order pixel. The pixelated noise ratio also tracks fairly well with spacing standard deviation, as shown in Figure 10.

An alternative way to compare the same grids is to use a larger pixel size. Figure 11 shows that, if a 3.9x larger pixel size is used, the performance of the randomized square grid does not improve as much with more randomization – the improvement is only 2.3, resulting in a pixel with a signal of only 0.53% of the signal in the zero-order pixel. This is because, as the pixel size increases, more of the spread-out diffracted energy is contained within a pixel. Another major difference in simulations that use larger pixel sizes is that the variation of the line spacing no longer predicts the diffracted performance as well.

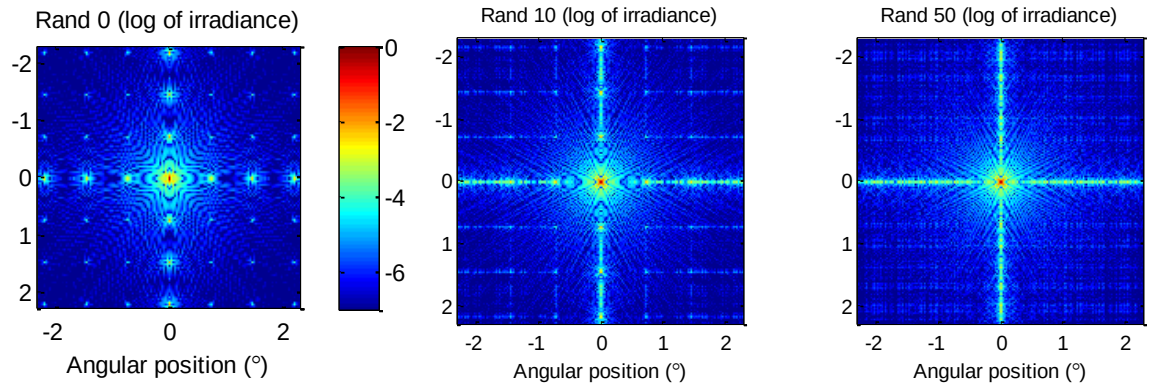

Figure 8 Randomization of a square grid (0% through 50% randomization) spreads the energy from the higher-order diffraction peaks, but only does so along a horizontal and vertical line from the original diffraction peak.

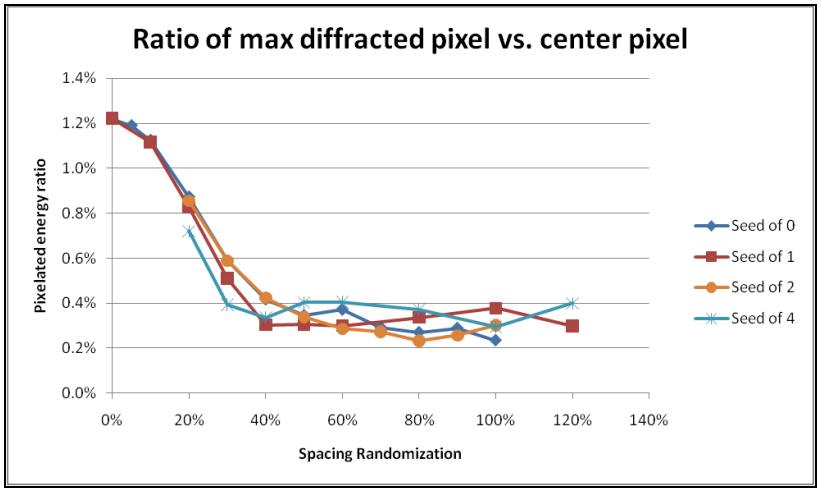

Figure 9 Quantitative comparison of randomized square grids using the noise metric with pixels equal to the Airy disk size. All cases shown have g = 50µm, 2a = 5µm, λ = 0.6328µm, and a sheet resistance of 10 Ω/□.

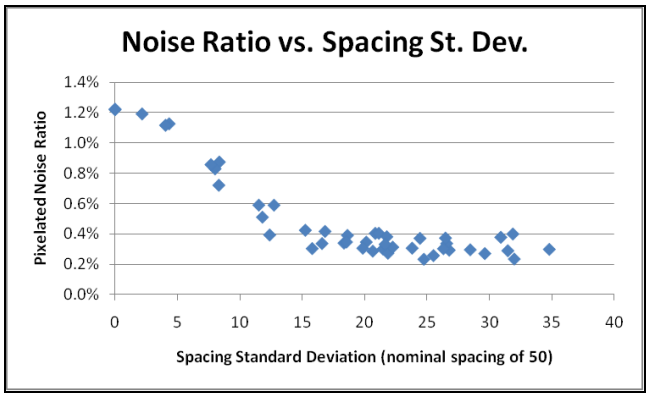

Figure 10 For small pixel sizes, the pixelated metric tracks well with the spacing variation.

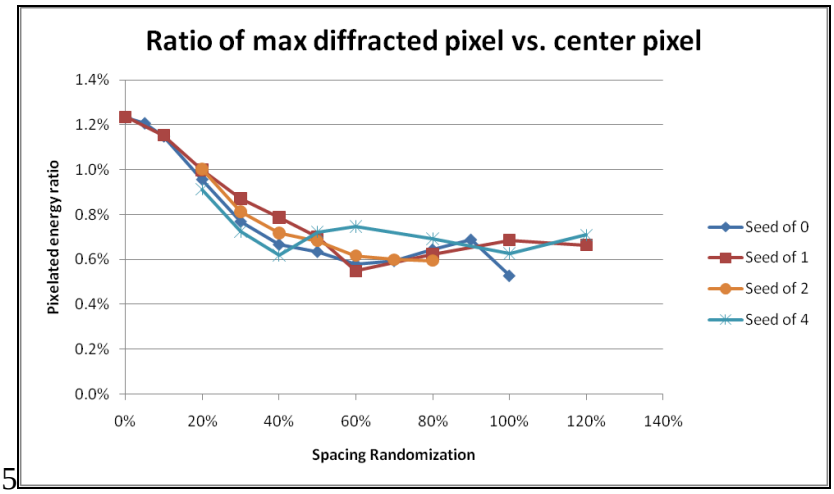

5

Figure 11 Quantitative comparison of randomized square grids using pixels equal to half of the distance from the zero-order peak to the first diffracted peak. For the grids analyzed in this figure, this is a 3.9x larger pixel size. All cases shown have g = 50μm, 2a = 5μm, λ = 0.6328μm, and sheet resistance of 10 Ω/□.

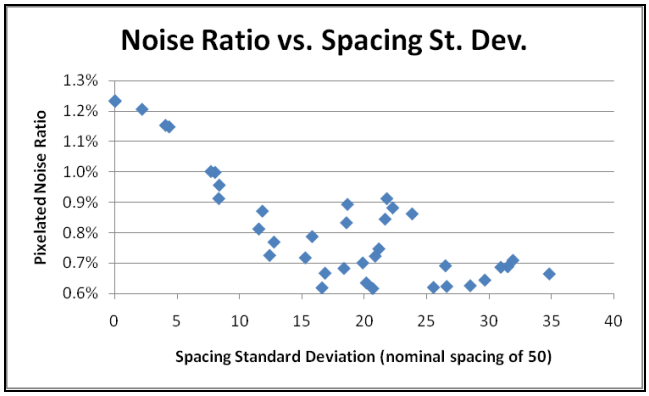

Figure 12 For larger pixel sizes, the pixelated metric does not track as well with the spacing variation.

3.2 Hub-and-spoke diffraction

One of the first decisions about what type of hub-and-spoke pattern to use is the ratio between the circle (hub) diameters and the spacing between the hubs. Figure 13 shows that the ratio has a significant effect on even energy distribution, and that the previously published ratio of 1.6 is not ideal for minimizing diffraction. Figure 14 and Figure 15 show the difference in diffraction patterns from the 1.6 ratio and 2.5 ratio cases.

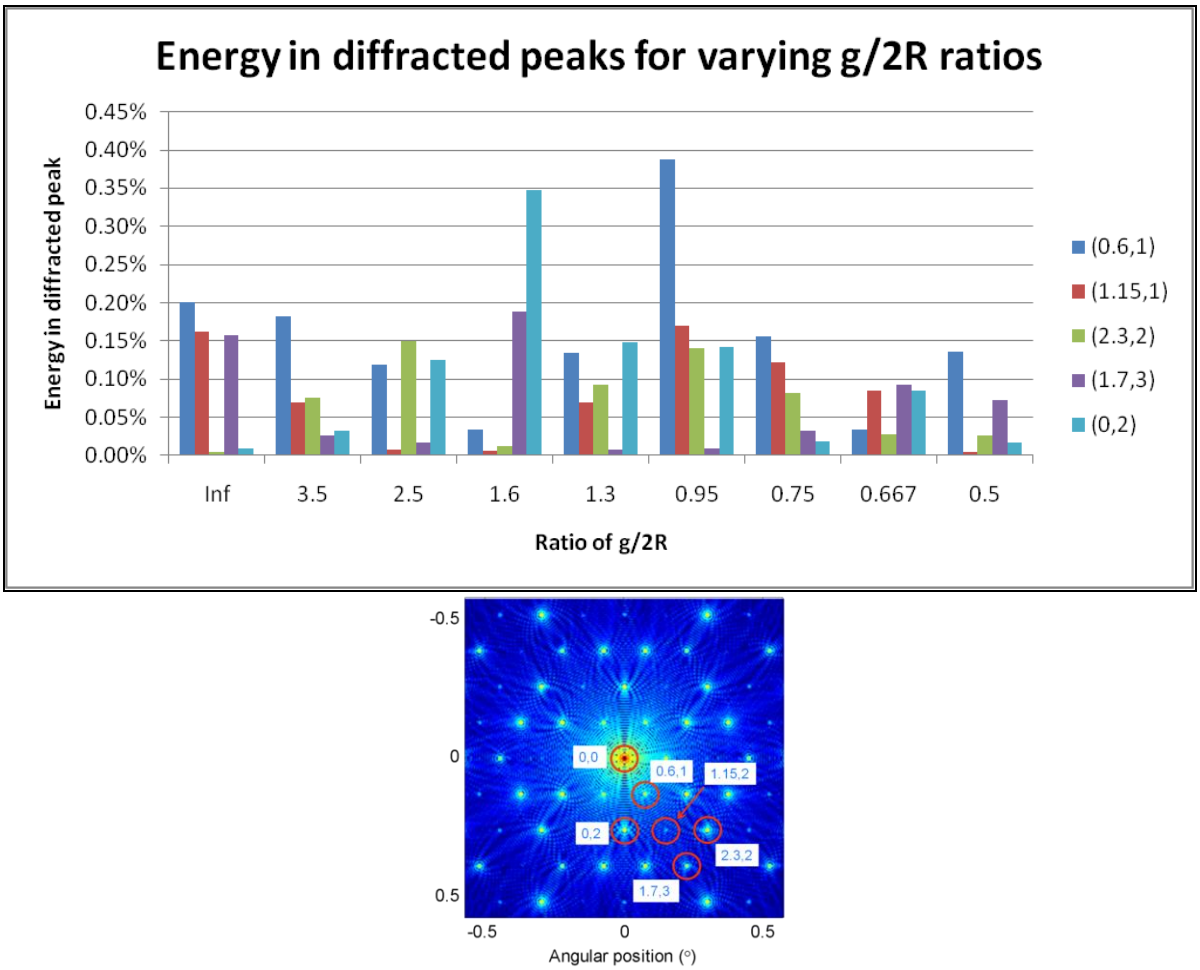

Figure 13 Comparison of the energy levels in diffracted peaks for grids with varying g/2R ratios (top) and the naming convention used to describe peaks (bottom). Note that g/2R ratios below 1 correspond to overlapping circle patterns (see next section).

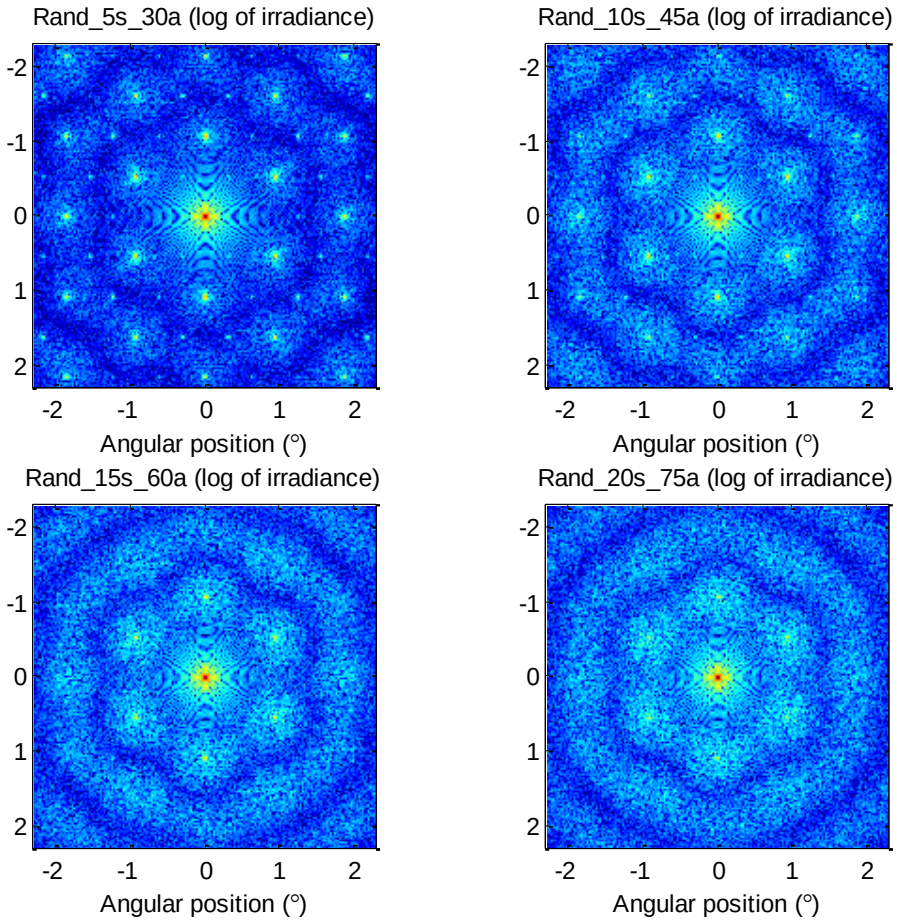

Figure 14 Increasing spoke angle (30-75°) and hub spacing (5-20%) randomization for a g/2R ratio of 1.6 (g = 67.5μm, 2R = 42.2μm, 2a = 4μm, λ = 0.6328μm, sheet resistance of 10.0 Ω/□). The most random case reduces the energy in the (0,2) peak from 0.76% without randomization to 0.24%.

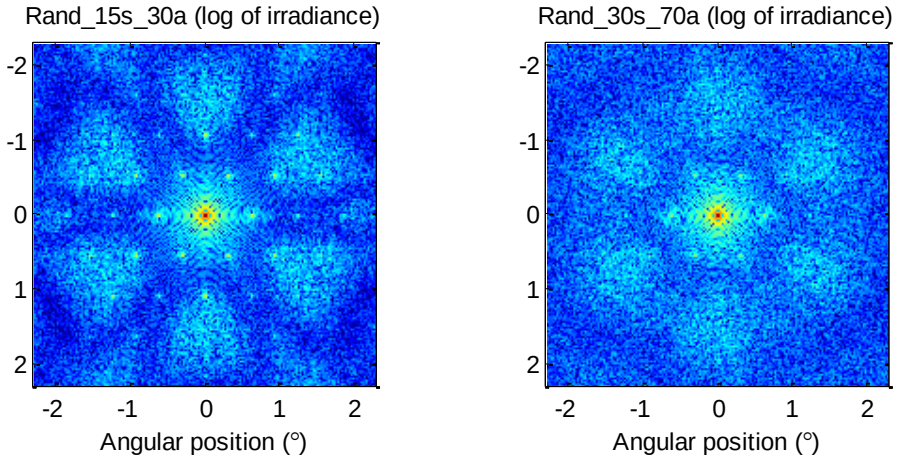

Figure 15 Increasing spoke angle (30-70°) and hub spacing (15-30%) randomization for a g/2R ratio of 2.5 (g = 67.5μm, 2R = 51.92μm, 2a = 4.04μm, λ = 0.6328μm, sheet resistance of 10.0 Ω/□). The most random case reduces the maximum diffracted energy to 0.11% , which is about half of the 0.24% of the 1.6 ratio case.

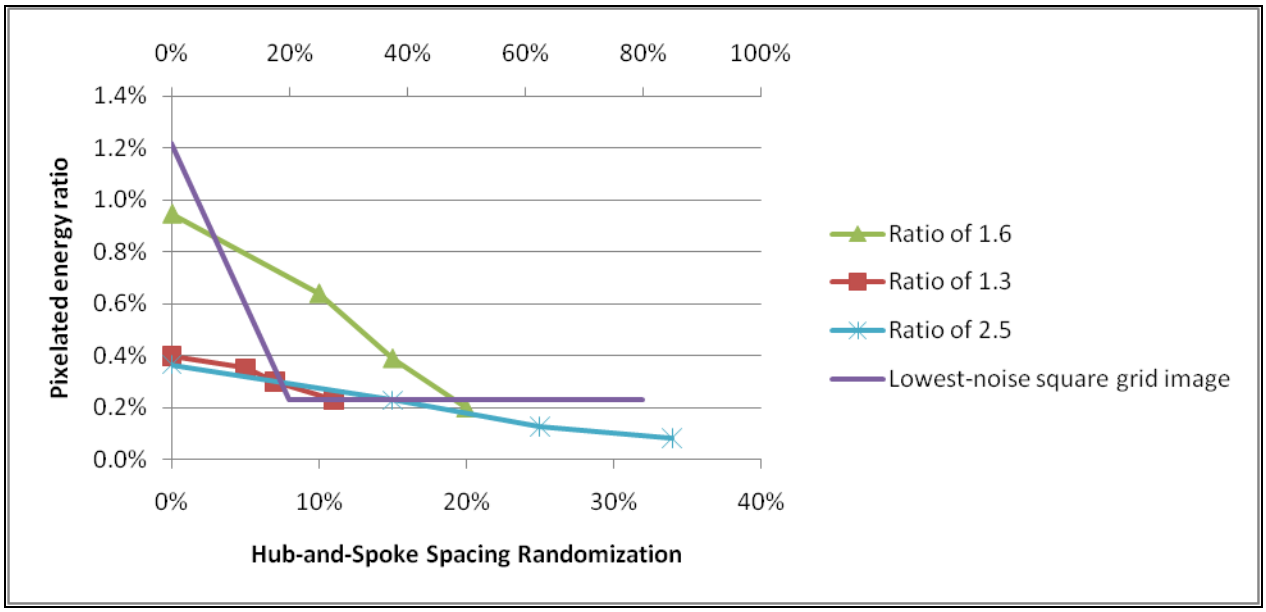

Figure 16 Noise metric performance (pixel equal to Airy disk diameter) of hub-and-spoke grids with varying g/2R ratios compared to square grid results. For simplicity, only the lowest-performing square grid results are shown.

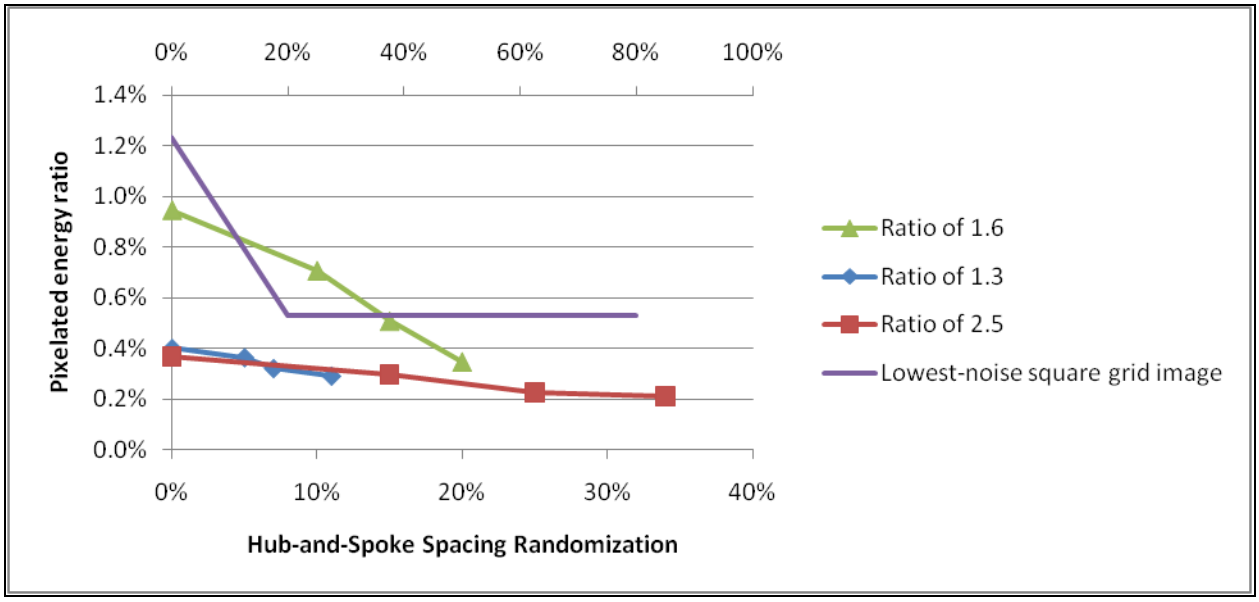

Figure 17 Noise metric performance (pixel equal to half of the distance to the first diffraction peak) of hub-and-spoke grids with varying g/2R ratios compared to square grid results. For simplicity, only the lowest-performing square grid results are shown.

3.3 Overlapping circle diffraction

Overlapping circles can be considered as hub-and-spoke patterns where the hub diameter is greater than the spacing between hubs. As was seen in Figure 13 above, a g/2R ratio of 2/3 most evenly distributes the energy between the different diffraction orders, which is evident in Figure 23 below. One of the advantages of using overlapping circle patterns is that the hub diameter can be easily randomized, adding an additional variable for randomization. The result of randomizing spacing and hub diameter is shown in Figure 24 – there is no longer a discernable diffraction pattern.

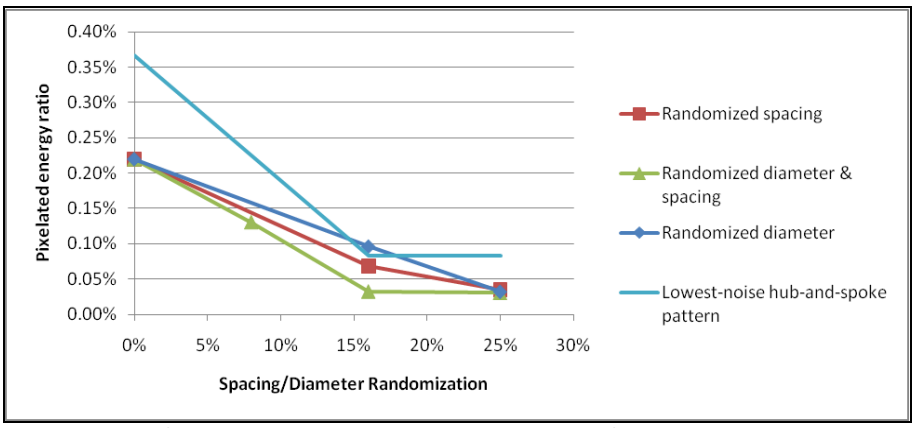

Figure 18 Noise metric performance (pixel equal to Airy disk diameter) of overlapping grids with a g/2R ratio of 2/3 compared to hub-and-spoke results. The most random overlapping circle pattern decreases the repeating noise by 40% and the randomized noise by 64% when compared to the best hub-and-spoke case. For simplicity, only the lowest-performing hub-and-spoke grid results are shown.

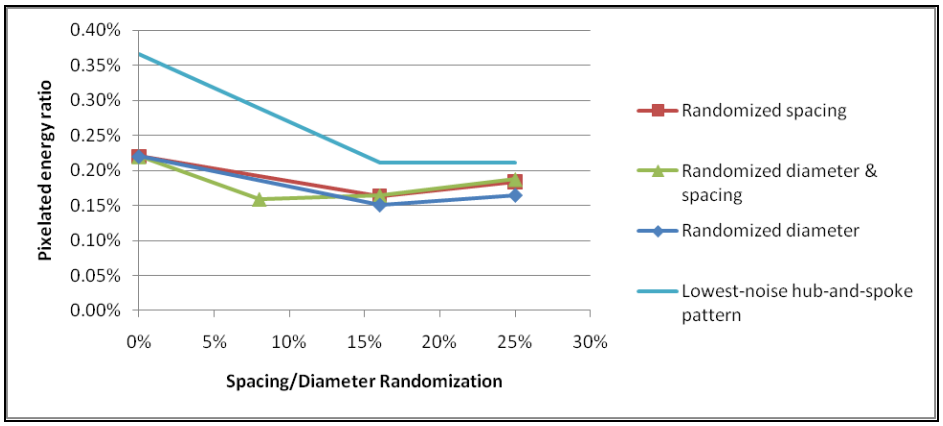

Figure 19 Noise metric performance (pixel equal to half of the distance to the first diffraction peak) of overlapping grids with a g/2R ratio of 2/3. The most random overlapping circle pattern decreases the repeating noise by 40% and the randomized noise by 29% when compared to the best hub-and-spoke case. For simplicity, only the lowest-performing hub-and-spoke grid results are shown.

4. MEASUREMENTS

Transmission of a set of samples was measured at normal incidence using a 4mm diameter beam with a camera focused on the central diffraction pattern. A measurement of the un-attenuated (0,0) peak was first obtained, followed by a measurement with the peak removed to allow a comparison of the diffracted energy relative to the central peak. A wavelength of 533nm was used to allow digital camera images of the large-scale diffraction pattern. The resulting patterns matched modeled patterns extremely well (see Figure 21 through Figure 24).

Transmission predicted using open area squared matched measured transmission to better than 2% after correcting for substrate transmission and Fresnel reflection losses (see Figure 20). A number of linewidth measurements were made on the samples in the figure with a measurement uncertainty of 0.1µm relative to the 2-8 µm linewidths.

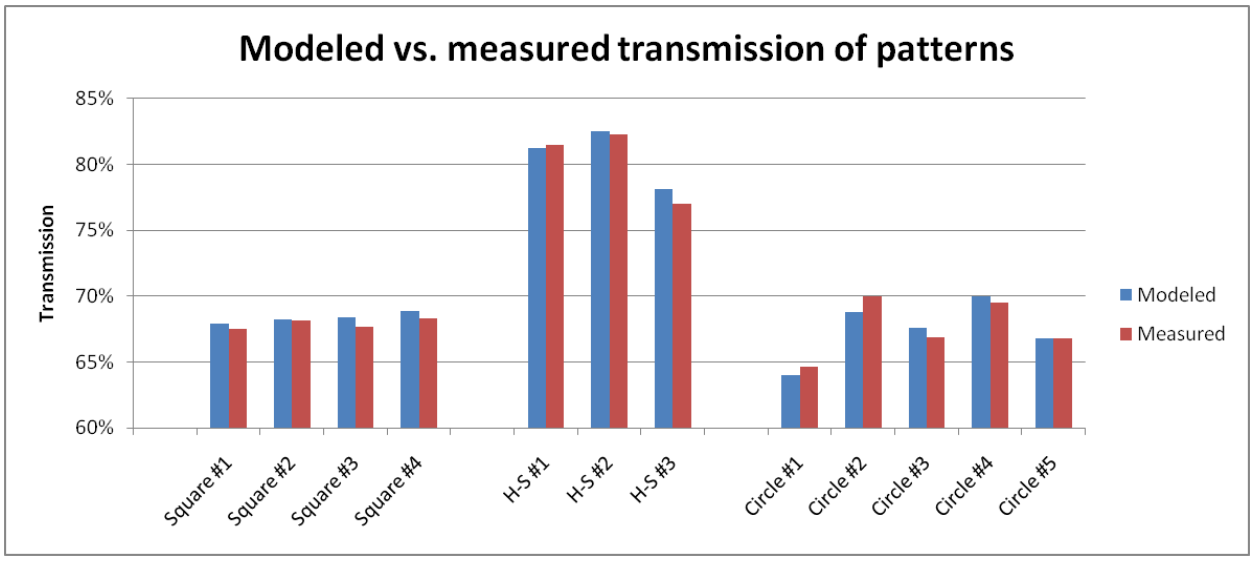

Figure 20 Modeled and measured transmission through repeating and randomized grids. Differences between patterns are due to line width variations, and do not reflect inherent limitations of pattern types.

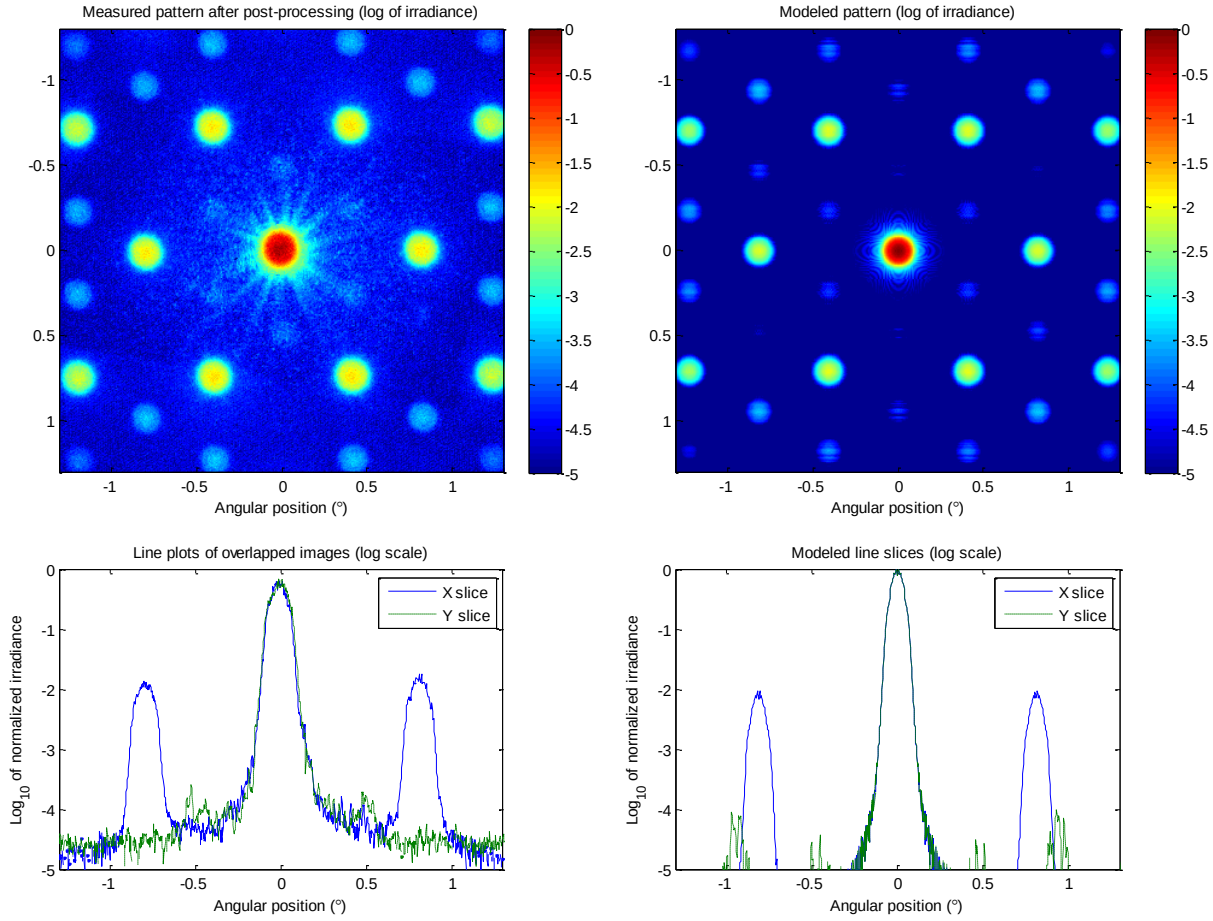

Figure 21 Transmission through a repeating hub-and-spoke grid with a g/2R ratio of 1.6.

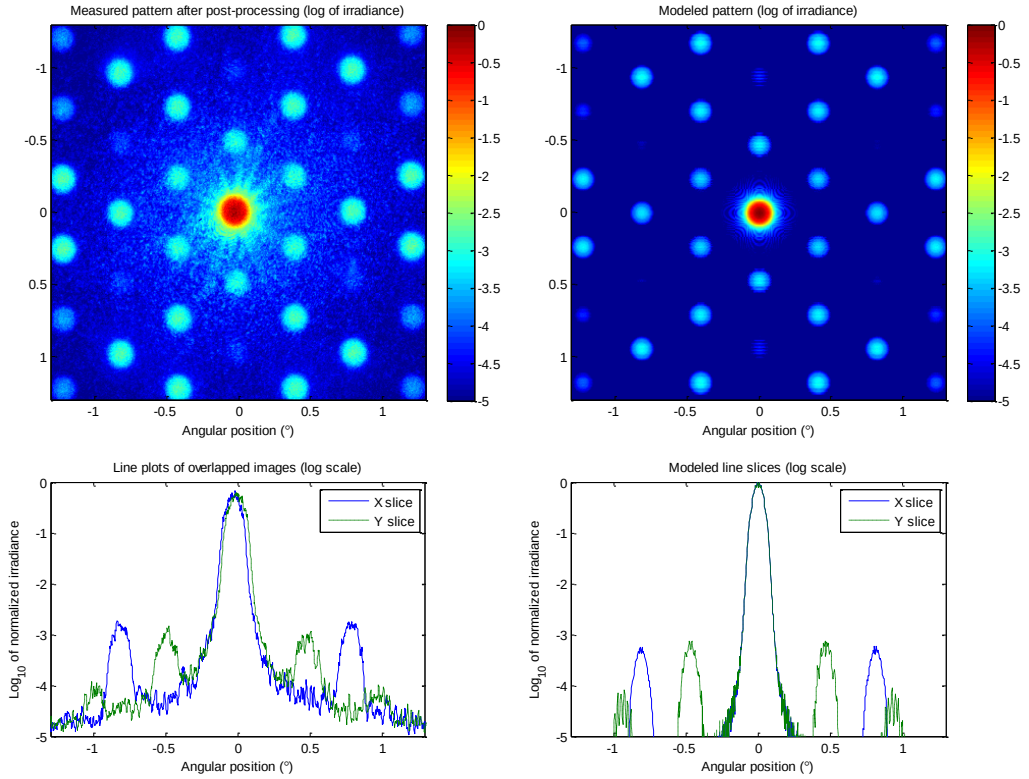

Figure 22 Transmission through a repeating hub-and-spoke grid with a g/2R ratio of 2.5.

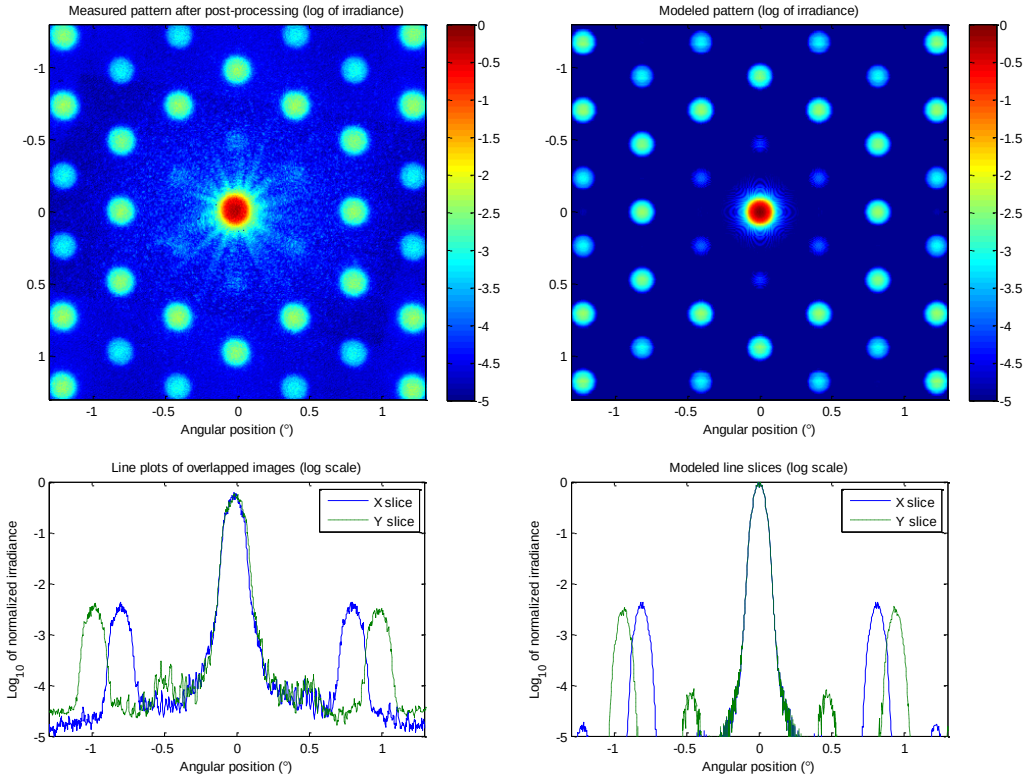

Figure 23 Transmission through a repeating overlapping grid with a g/2R ratio of 2/3.

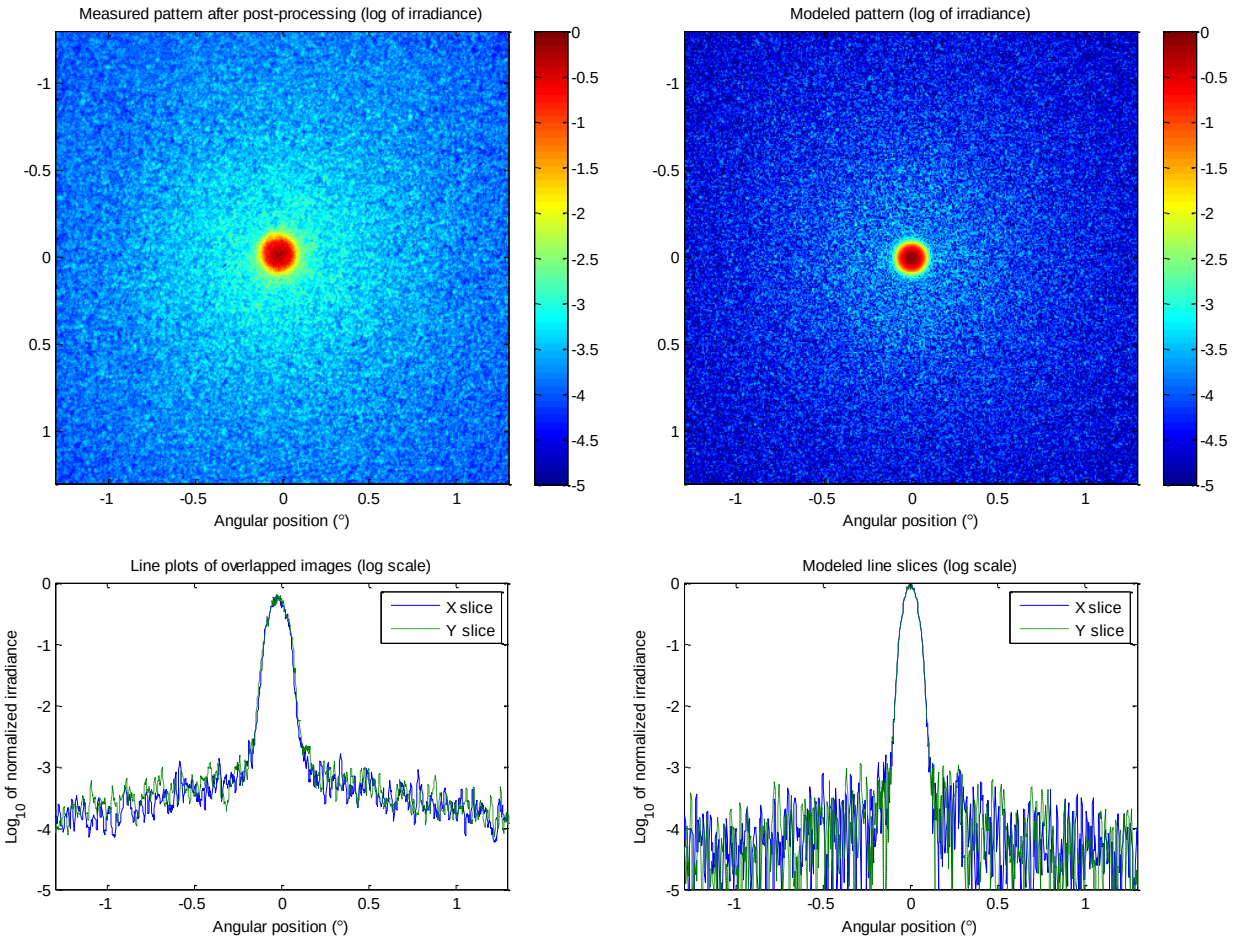

Figure 24 Transmission through a randomized overlapping grid with a g/2R ratio of 2/3 using 20% spacing and 20% diameter randomization.

5. CONCLUSION

The purpose of this study was to investigate the diffraction from various types of patterns and determine which patterns can be used to minimize energy in unwanted diffraction orders. Existing OptiScan diffraction propagation software was enhanced by the University of Arizona's Milster Group to add a Babinet approach for calculating diffraction from an arbitrary input. The final algorithm has been tested against previously published papers, which included analytically-derived as well as measured results.

The modeled OptiScan results qualitatively and quantitatively match referenced literature within the assumptions and test errors of the references, and the algorithm is shown to be reliable for predicting both locations and energies of diffracted peaks. Measurements of samples demonstrated the accuracy of modeling repeating and randomized patterns of all types.

As shown in Figure 25, the diffraction peaks of different pattern types vary significantly before and after randomization, and diffraction of a repeating pattern is a good predictor of diffraction with randomization. If a simple mask and low inspection time are important, a randomized square pattern is a good solution. If circular patterns are not an issue, a hub-and-spoke pattern can have good performance, although the standard reported pattern type (g/2R ratio of 1.6) does not have the best performance (a *repeating* pattern with a g/2R ratio of 2.5 has nearly the same performance with large pixels as a *randomized* hub-and-spoke pattern with a g/2R ratio of 1.6, and when randomized has significantly better performance). An overlapping circle pattern provides the best diffraction performance in all cases, although the transmission of a repeating overlapping circle is less than that of a square or hub-and-spoke pattern with equivalent sheet resistance.

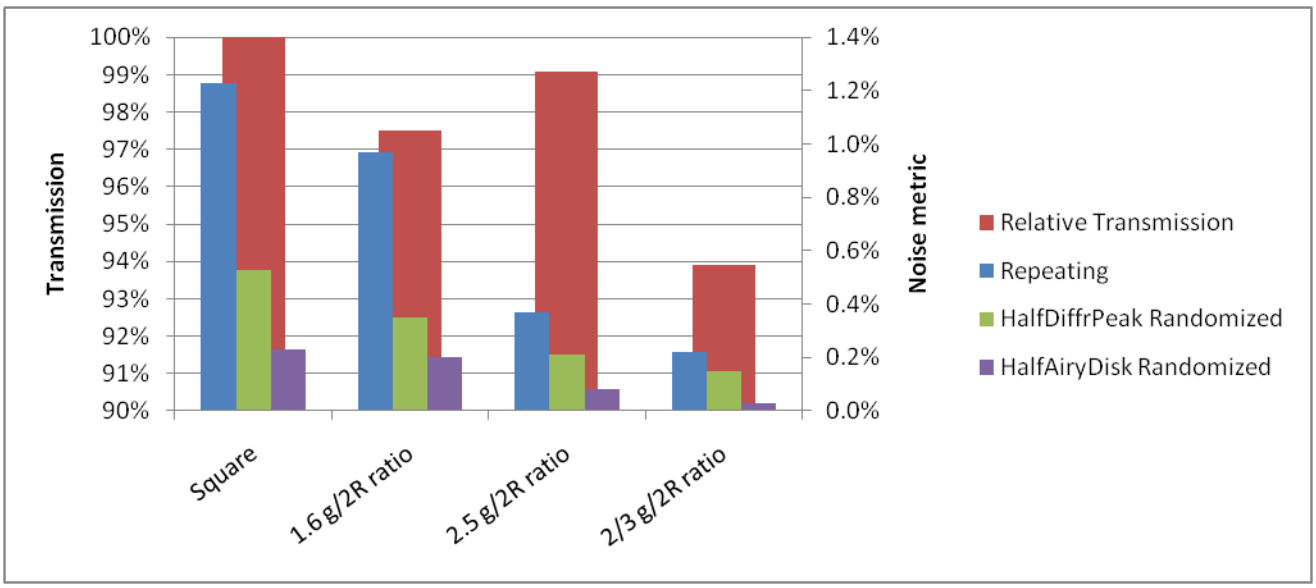

Figure 25 Summary of the noise metric and transmission for different pattern types with the same patterned sheet resistance. Square grids have the highest transmission but have a higher diffracted signal with and without randomization. Hub-and-spoke patterns balance transmission and randomization, especially when a spacing/diameter ratio of 2.5 is used. Overlapping circle patterns have low transmission, but have similar diffraction performance as hub-and-spoke patterns even without randomization, and with spacing and diameter randomization spread diffracted light very uniformly.

ACKNOWLEDGEMENTS

This work was partially sponsored by the Air Force Research Laboratory (AFRL) under Contract Nos. FA 8650-06-D-5401/0012, FA 8650-06-D-5401/0014, and FA 8650-05-D-5806/0012. The authors would also like to acknowledge others who created the masks and grid patterns, including Tony DiBiase, Bryan Guerre, and Ricardo Marroquin from Exotic Electro-Optics and Steph Perry, David Casale, and Carmen Barone from Max Levy Autograph, as well as Michael Thomas and Andrew Griffin from Spica Technologies for their creativity in testing the patterns.

REFERENCES

[1] Kohin, M., Wein, S. J., Traylor, J. D., Chase, R. C. and Chapman, J. E., “Analysis and design of transparent conductive coatings and filters,” Opt. Eng. 32(5), 911-925 (1993).
[2] Jacoby, K., Pieratt, M.W., Halman, J. I. and Ramsey, K. I., “Predicted and measured EMI shielding effectiveness of a metallic mesh coating on a sapphire window over a broad frequency range”, Proc. SPIE 7302, 73020X (2009).
[3] Halman, J. I., Ramsey, K. I., Thomas, M. and Griffin, A., “Predicted and measured transmission and diffraction by a metallic mesh coating,” Proc. SPIE 7302, 73020Y (2009).
[4] Tan, J. and Lu, Z., "Contiguous metallic rings: an inductive mesh with high transmissivity, strong electromagnetic shielding, and uniformly distributed stray light," Opt. Express 15(3), 790-796 (2007).
[5] Tan, J. and Lu, Z., “Analysis of transmitting characteristics of high-transparency double-layer metallic meshes with submillimeter period using an analytical model”, Appl. Opt. 47(29), 5519-5526 (2008).
[6] Pieratt, M., Murray, I., Hibbard, D., “Improved Transmission and Sheet Resistance Modeling for Grid Patterns,” Proc. 13th DoD EMWS, (2010).
[7] Lang, M. and Milster, T., “Investigation of optics in the 10-200 μm size regime,” Opt. Review 14(4), 189-193 (2007).